Catal Lett (2009) 130:496–503
DOI 10.1007/s10562-009-9938-6

Photo Catalytic Degradation of Imidachloprid Under Solar Light Using Metal Ion Doped TiO_2 Nano Particles: Influence of Oxidation State and Electronic Configuration of Dopants

L. Gomathi Devi · B. Narasimha Murhty · S. Girish Kumar

Received: 22 December 2008 / Accepted: 11 March 2009 / Published online: 27 March 2009

Abstract Anatase TiO_2 was doped with metal ions like Th^{4+}, V^{5+} and Mo^{6+} and tested for the degradation of imidachloprid under solar light. X-ray diffraction results inferred that all the dopants stabilized the anatase phase irrespective of their nature, oxidation state and ionic size. The undoped and transition metal ion doped TiO_2 were completely transformed to rutile phase at 700 °C while rare earth Th^{4+} doped sample completely transformed to rutile phase at 1,000 °C. The rare earth dopant stabilized the anatase phase by hindering the growth of crystallite size. Among the photo catalysts used, Th^{4+} (0.06%)-TiO_2 showed highest activity and its efficiency was 2.8 times higher than that of Degussa P-25. The Th^{4+} ion lowered the band gap of TiO_2 to 2.6 and 2.5 eV facilitating solar light absorption. Detrapping of the trapped charge carriers depends on electronic configuration and the oxidation state of the dopants.

Keywords Stabilization of anatase phase in TiO_2 · Th^{4+} doping · V^{5+} and Mo^{6+} doping · Imidachloprid · Photodegradation under solar light

1 Introduction

Applications to photo catalytic degradation of organic contaminants using TiO_2 has been extensively studied [1–3]. TiO_2 is mainly used because of its low cost, high catalytic activity, non toxicity, physical and chemical stability. The high degree of recombination between photo generated electrons and holes is a major limiting factor controlling the photo catalytic efficiency. Further, TiO_2 being the poor absorbers of photons in the visible region, its activation under solar light is difficult due to its broad band gap. Band gap tailoring by doping with appropriate cations is the most efficient and frequently used method. Doping with metal ions (transition and inner transition) serves to prolong the separation of charge carriers and also extends the absorption band to the visible region [3, 4]. In addition, doping with lanthanide ions increases the adsorptive capacity of the catalyst surface by forming complex between the functional group of organic pollutants and 'f' orbital of the dopant. Although doping of inner transition metals with '4f' series is extensively reported [5–7], least attempt is made with '5f' series elements. To the best of our knowledge, photo catalytic activity of the doped catalysts under solar light correlating with oxidation state and electronic configuration of the dopant is not reported. In this view the present research mainly aims at

1. Extending the TiO_2 response to the visible region by doping with transition metal ions (V^{5+} and Mo^{6+}) and inner transition metal ion (Th^{4+}).
2. Role of dopants inside the TiO_2 matrix considering its oxidation state and electronic configuration.
3. The photo catalytic activity of these catalysts were tested for the degradation of imidachloprid (IMC) under solar light and compared with the commercially available Degussa P-25.

2 Experimental Section

2.1 Chemicals

Titanium tetrachloride [$TiCl_4$], ammonium vanadate [NH_4VO_3] and ammonium molybdate [$(NH_4)_6Mo_7O_{24}{\cdot}4H_2O$] were

L. Gomathi Devi (✉) · B. Narasimha Murhty · S. Girish Kumar
Department of Post Graduate Studies in Chemistry, Bangalore University, Central College City Campus, Bangalore 560001, India
e-mail: gomatidevi_naik@yahoo.co.in

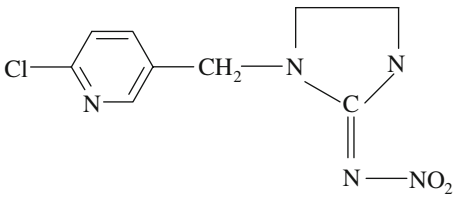

Fig. 1 Structure of Imidachloprid

supplied from Merck Chemicals. Thorium nitrate [$Th(NO_3)_4$], were obtained from Sisco-Chem industries, Bombay. Imidachloprid pesticide was obtained from Rallies Research limited. The structure of the pesticide is shown in Fig. 1.

2.1.1 Photochemical Reactor

All the experiments were carried out using a borosilicate glass reactor (150 × 75 mm) with surface area of 176 cm^2 of one liter capacity. Photo catalysis using solar light was performed between 11 am and 2 pm during the summer season (May–June) in Bangalore, India. The latitude and longitude are 12.58 N and 77.38 E, respectively. The average intensity of sunlight was around 1,200 W cm^{-2}. The intensity of solar light was concentrated by convex lens and the reaction mixture was exposed to this concentrated solar light. In a typical experiment 400 mL of 10 ppm IMC solution along with 300 mg of the catalyst (sufficient to absorb maximum incident flux) was magnetically stirred for 30 min to attain adsorption equilibrium of pollutant on the surface of the catalyst. The solutions were periodically withdrawn and centrifuged to remove the catalyst nano particles and the centrifugate were analyzed by UV–visible spectroscopic analysis (using Shimadzu UV-1700 pharmaspec UV–visible spectrophotometer) to follow the degradation process.

2.1.2 Catalyst Preparation

Anatase TiO_2 was prepared by sol–gel method [8]. $Th(NO_3)_4$, NH_4VO_3 and $(NH_4)_2Mo_{27}O_{24}{\cdot}4H_2O$ were used as sources for doping Th^{4+}, V^{5+}, and Mo^{6+} into the TiO_2 lattice. The process involves the addition of known volume of metal ion solution to the calculated amount of anatase TiO_2 to get the concentration of dopants in the range of 0.02–0.1%. The mixture is thoroughly grinded in a mortar for 1 h and oven dried at 120 °C for 3–4 h. The process of heating and grinding is repeated four times to ensure the homogeneous distribution. The resulting photocatalyst powder is then calcined at 550 °C for 4.5 h [4].

2.1.3 Catalyst Characterization

The phase structure of the catalyst were analyzed by X-ray diffraction (XRD) technique using Philips powder diffractometer PW/1050/70/76 using Cu Kα radiation with 2θ scan rate of 2°/min. The crystallite size was calculated using Scherer's equation for a diffraction pattern recorded at a slow scanning speed of 1/2° per minute. Specific surface area of the photo catalyst was determined by Digisorb 2006 surface area, pore-volume analyzer-Nova Quanta Chrome Corporation instrument multipoint BET adsorption. The optical/electronic properties were analyzed by UVVisible diffuse reflectance spectrometer (Shimadzu, 3101 PC UV-VIS-NIR instrument) using $BaSO_4$ as reference standard. The surface morphology was studied by SEM using JSM 480 microscope operating at 25 kV on specimen upon which a thin layer of gold has been evaporated. EDX was employed to obtain the information on the amount and distribution of metal ion species in the samples.

3 Results and Discussions

3.1 XRD Analysis

The doped M-TiO_2 (M = Th^{4+}, V^{5+} and Mo^{6+}) samples showed only anatase phase similar to that of undoped TiO_2 irrespective of its oxidation states, ionic radii and also nature of metal ion. The influence of dopants on the structural properties can be explained by the changes caused by the dopants on the defect structures of TiO_2 matrix; these changes are strongly dependent on the charge and size of the dopant ion. The presence of only anatase phase in all the doped samples can be accounted in the following way.

1. The doping of cation with a charge greater or less than +4 into the TiO_2 lattice is expected to induce oxygen vacancies. These oxygen vacancies facilitate easier solid state rearrangement of the ions which results in lowering the temperature required for crystallization. The ionic radius of Th^{4+} is much larger than Ti^{4+}. Due to the large ionic radius, it is impossible for Th^{4+} ions to act as interstitial ions in the TiO_2 matrix. Therefore, the Th^{4+} can only replace Ti^{4+} ions substitutionally at the lattice sites. It is well known fact that anatase phase is thermodynamically stable phase for smaller crystallite size and phase transformation to rutile occurs only when the crystallite size exceeds the optimum value. It is expected that inner transition metal ions inhibit the phase transformation from anatase to rutile through the formation of Ti–O–M bond [9]. On the other hand, the ThO_2 lattice locks the Ti–O species at the interface with the TiO_2 domains preventing the nucleation necessary for phase transformation. The transition metal doped and pristine TiO_2 were completely

transformed to rutile phase at 700 °C, while the Th^{4+}-TiO_2 sample was completely transformed to rutile phase at the calcinations temperature of 1,000 °C. Thus it can be concluded that Th^{4+} in the present case effectively hinders the crystallite growth and increases the calcinations temperature for the phase transformation. Burns et al. [10] reported that Nd^{3+} ion occupies lattice positions of Ti at lower dopant concentration and interstitial site at higher dopant concentration (>0.1 mol%). In the line of this reasoning, the concentration of Th did not exceed 0.1%. Thus it can be proposed that Th^{4+} has occupied lattice positions of Ti in TiO_2. Since the ionic radius of the dopant is higher than the Ti^{4+}, its incorporation into the TiO_2 lattice induces oxygen vacancies at a close proximity (Th–Vo). These oxygen vacancies can be neutral or ionized. However, these oxygen vacancies are not sufficient to facilitate rutile phase transformation. Therefore nucleation of rutile phase is prevented resulting in the enhanced stability of anatase phase.

2. In the case of molybdenum it has been shown by ESR that Mo^{5+} and Mo^{6+} can coexist simultaneously during illumination [11]. The ionic size of V^{5+}, Mo^{6+}, and Mo^{5+} is almost similar to that of Ti^{4+}. Further introduction of vanadium and molybdenum should reduce the amount of oxygen vacancies due to the fact that these ions have higher positive charge than the host ion leading to the hindering of anatase to rutile phase transformation. These results show that all the dopants substitute Ti^{4+} in TiO_2 lattice without distorting the crystal structure.

3.2 Calculation of Lattice Parameters

The average grain size calculated using Scherer's equation from the width of hundred percent intense (101) reflection for all the photo catalysts are listed in Table 1. The results showed that doped M-TiO_2 (Th^{4+}, V^{5+}, and Mo^{6+}) showed a decrease in their crystallite size compared to undoped TiO_2.

Table 1 Detailed characterization of all the photo catalysts used in the study

Photo catalyst	Lattice parameters Å	Unit cell volume $(Å)^3$	Crystallite size nm	Surface area m^2/g	Band gap eV
TiO_2	3.7828 ± 0.0003	135.97	26.34	18	3.1
(0.00%)	9.5023 ± 0.0005				
Th^{4+}-TiO_2	3.7822 ± 0.0006	136.07	24.28	26	2.8
(0.02%)	9.5123 ± 0.0013				
Th^{4+}-TiO_2	3.7826 ± 0.0008	136.34	24.29	34	2.6 & 2.5
(0.06%)	9.5293 ± 0.0004				
Th^{4+}-TiO_2	3.7814 ± 0.0006	136.27	30.28	32	3.0
(0.10%)	9.5301 ± 0.0012				
V^{5+}-TiO_2	3.7822 ± 0.0004	136.05	26.24	23	2.9
(0.02%)	9.5113 ± 0.0007				
V^{5+}-TiO_2	3.7824 ± 0.0009	136.10	26.30	26	2.6
(0.06%)	9.5136 ± 0.0005				
V^{5+}-TiO_2	3.7825 ± 0.0006	136.13	28.42	24	2.7
(0.10%)	9.5152 ± 0.0007				
Mo^{6+}-TiO_2	3.7801 ± 0.0009	136.04	26.28	25	2.9
(0.02%)	9.5209 ± 0.0005				
Mo^{6+}-TiO_2	3.7801 ± 0.0008	136.32	26.40	28	2.5
(0.06%)	9.5406 ± 0.0002				
Mo^{6+}-TiO_2	3.7809 ± 0.0003	136.10	29.38	22	2.7
(0.10%)	9.5212 ± 0.0004				

The crystallite size was calculated from Scherrer's equation: $D = k\lambda/\beta\cos\theta$, D is the crystallite size, k is the constant (shape factor, about 0.9), λ is the X-ray wavelength (0.15418 nm), β is the full width at half maximum (FWHM) of the diffraction line and θ is the diffraction angle. The values of β and θ are taken from crystal plane (101) of anatase phase

Lattice parameters was calculated using $\frac{1}{d_{hkl}^2} = \frac{h^2+k^2}{a^2} + \frac{l^2}{c^2}$, d_{hkl} is the distance between crystal planes of (hkl), λ is the X-ray wavelength, θ is the diffraction angle of crystal plane (hkl), hkl is the crystal plane index and a, b, c are the lattice parameters

Surface area are measured from BET analysis

Band gap was calculated from Kubelka Munk plot of $(1-R_\infty)^2/2R_\infty$ vs. wavelength

This was attributed to the formation of M–O–Ti bond in the doped samples which inhibits the growth of crystal grains. The crystallite size of Th^{4+}-TiO_2 is smaller compared to V^{5+}-TiO_2 and Mo-TiO_2 samples. This may be due to the effective anatase phase stabilization by Th^{4+} ions by hindering crystallite growth compared to V^{5+}-TiO_2 and Mo^{6+}-TiO_2 samples. On doping with metal cations (Th^{4+}, V^{5+}, and Mo^{6+}), diffraction angles of the crystal plane (101) of anatase shifts to higher angles confirming the incorporation of metal cations into TiO_2 matrix. This shift is higher for Th^{4+} substitution compared to V^{5+} and Mo^{6+} dopants which may be due to the higher ionic size of the Th^{4+} ions (0.095 nm). This is further confirmed by lattice parameters showing elongation along c-axis for Th^{4+}-TiO_2 samples compared to other Mo^{6+}-TiO_2 and V^{5+}-TiO_2 samples. Due to similarity in the ionic size of Mo^{6+} (0.062 nm) and V^{5+} (0.059 nm) with that of Ti^{4+} (0.068 nm) it can be easily substituted into the TiO_2 lattice at Ti lattice position which is further confirmed by the Vegards's law (Change in the unit cell dimension should be linear with change in the dopant composition) confirming the possibility of incorporation of the metal ions as a substituent in TiO_2 lattice [4]. The variation in lattice parameter and also increase in the unit cell volume of doped samples compared to undoped TiO_2 confirms the incorporation of dopant into the TiO_2 matrix. At higher dopant concentrations (≥0.1%), the excess dopant ions may not enter the TiO_2 lattice leading to the slight decrease in the unit cell volume. The observed unit cell volume is still higher than the undoped TiO_2. This may happen by pushing the extra atoms towards the interstitial sites. Further the atoms at the regular site may be missing from their relative positions. These imperfections may lead to the reduction in the unit cell volume at higher dopant concentrations.

3.3 UV–Visible and Diffuse Reflectance Spectral Studies

Sanchez and Lopez [12] suggested that small band gaps were caused by stoichiometric deficiency of Ti/O ratios. The intensity of the reflected radiation provides information about the wavelength at which semiconductor absorbs the light. A plot of $(1-R_\infty)^2/2R_\infty$ (relative reflective intensity) versus wavelength is referred to as Kubelka–Munk plot, where R_∞ is the ratio of relative reflected intensity of the sample to that of non-absorbing standard ($BaSO_4$). R_∞ is the values obtained from the spectra at various wavelengths. $(1-R_\infty)^2$ is the molar absorption coefficient and $2R_\infty$ is the scattering coefficient. These plots are shown in Fig. 2a–d. The tangent to linear portion of the curve intersects the wavelength axis. Using this wavelength value band gap of

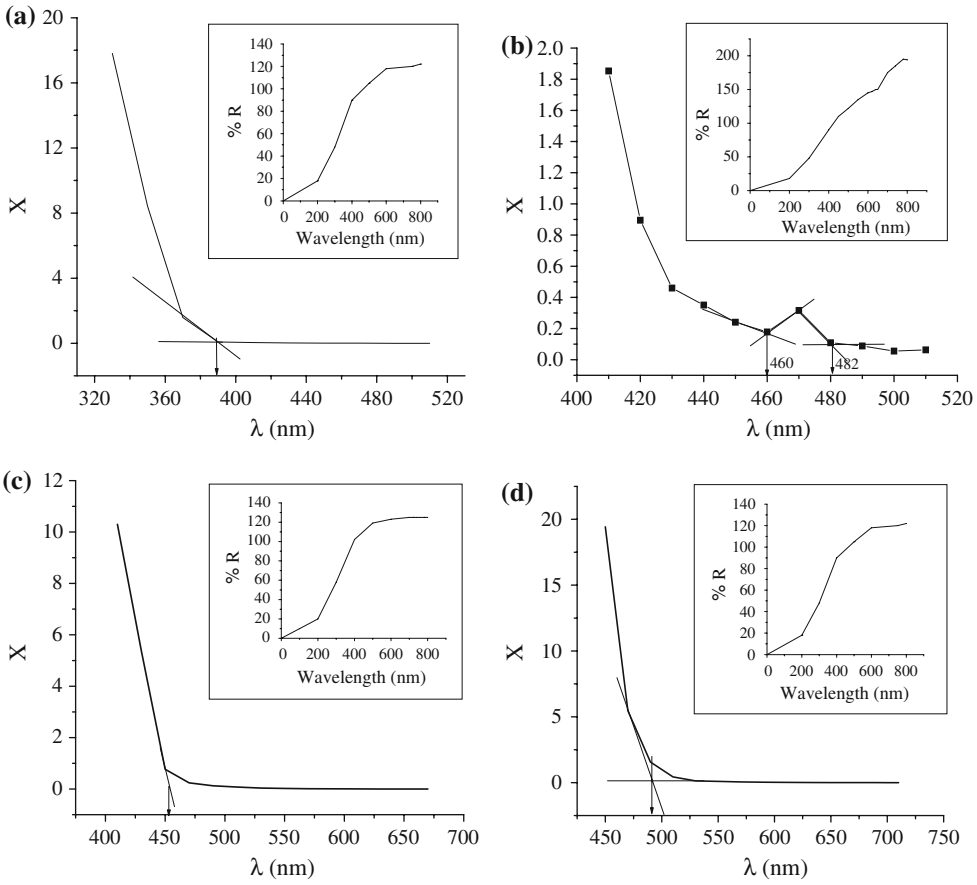

Fig. 2 Kubelka–Munk plot of X vs. wavelength where $X = (1-R_\infty)^2/2R_\infty$. The *inset* in the figure refers to the diffused reflectance spectra (*DRS*) of the respective catalyst. **a** Undoped TiO_2; **b** Th^{4+} (0.06%)-TiO_2; **c** V^{5+} (0.06%)-TiO_2; **d** Mo^{6+} (0.06%)-TiO_2

the photocatalyst is calculated. All the doped samples showed shift in the absorption to the longer wavelength. The extents of red shift were dependent on the dopant concentration and also on the nature of the dopants. The incorporation of dopants significantly reduced the band gap by creating mid band gap states ~2.6 and 2.5 eV. These results provide a clear evidence for the narrowing of band gap energy by cation substitution which endows the doped samples with visible light harvesting capacity. The band structure in undoped TiO_2 consists of metal 3d level and O 2p level which forms conduction band and valence band, respectively. The substitution of *n*-type dopants V^{+5} and Mo^{+6} in TiO_2 lattice are expected to form the impurity level just below the conduction band. Mo substitution shows red shifts to an extent of 480 nm which is slightly greater than V substitution that shows red shift to 450 nm. This difference could be attributed to the electronegativity of the metal atom. The substituted Mo (1.8) which is more electronegative than V (1.5) and also 4d level of Mo states are expected to have lower energy than 3d level of V taking into account that energy of the electronic energy level is inversely proportional to its electronegativity [13]. This results in the position of impurity level of Mo just below the impurity level of V. Hence the band gap absorption in the visible region for the V^{5+}-TiO_2 and Mo^{6+}-TiO_2 samples corresponds to electronic transition between 3d and 4d level of V and Mo to the band gap states of TiO_2. The Th^{4+}-TiO_2 samples showed two absorption bands at 466 and 486 nm in contrast to V^{+5}-TiO_2 and Mo^{6+}-TiO_2 samples which had one absorption band in the visible region. The electro negativity of Th (1.3) is almost similar to that of Ti (1.4). Hence impurity levels due to Th^{4+} substitution are expected to have same energy as that of V^{5+}. But the 6d level of Th^{4+} has lower energy as it is less shielded from the nucleus compared to the 3d level of vanadium. Hence a slight increase in the absorption at 466 nm is observed in contrast to vanadium which shows absorption band at 450 nm. The band at 466 nm in the case of Th^{4+}-TiO_2 samples is attributed to the electronic transition between 6d level of Th and band gap states of TiO_2 (Fig. 2a–d). The presence of Ti^{3+} ions in TiO_2 lattice cannot be ruled out, as Ti^{3+} states are expected to show absorption band nearly at 490 nm. The band at 486 nm may be probably due to the transition between 6f level of Th and 3d level of Ti. Further large red shift in the band gap of Th^{4+}-TiO_2 samples can also be due to its smaller crystallite size.

3.4 Defect Reactions of Dopants in TiO_2 Lattice

The mechanisms involved are complex and it is often difficult to predict the exact role of dopants in TiO_2 matrix. A probable mechanism of incorporation of these dopants is explained in accordance with Krogner–Vink notation.

If the incorporation of dopants creates conduction band electrons

$$V_2O_5 \leftrightarrow 2V_{Ti}^{\bullet} + 2e^- + 4Oo + \frac{1}{2}O_2 \quad (1)$$

$$Mo_2O_6 \leftrightarrow 2Mo_{Ti}^{\bullet\bullet} + 4Oo + 4e^- + O_2 \quad (2)$$

If the incorporation of dopants inducing interstitial oxygen which is less probable

$$V_2O_5 \leftrightarrow 2V_{Ti}^{\bullet\bullet} + O_i'' + 4Oo \quad (3)$$

$$Mo_2O_6 \leftrightarrow 2Mo_{Ti}^{\bullet\bullet} + 2O_i'' + 4Oo \quad (4)$$

If oxides are completely soluble then the dopant occupies substitution site leading to the creation of oxygen vacancies

$$V_2O_5 \leftrightarrow 2V_{Ti}^{\bullet\bullet} + Vo^{\bullet\bullet}/2V_o^{\bullet} + 5Oo \quad (5)$$

$$Mo_2O_6 \leftrightarrow 2Mo_{Ti}^{\bullet\bullet} + 2Vo^{\bullet\bullet}/4V_o^{\bullet} + 6Oo \quad (6)$$

The imbalance in the charge created on doping can also be compensated by titanium vacancies

$$2V_2O_5 \leftrightarrow 4V_{Ti}^{\bullet} + V_{Ti}'''' + 10Oo \quad (7)$$

$$2Mo_2O_6 \leftrightarrow 4Mo_{Ti}^{\bullet\bullet} + 2V_{Ti}'''' + 12Oo \quad (8)$$

Due to absence of charge imbalance in the case of Th^{4+} dopant ions, the above reactions are not possible and only reaction possible is inducing doubly ionized oxygen vacancies in the lattice owing to its larger ionic size.

$$ThO_2 \leftrightarrow Th_{Ti} + Oo + Vo^{\bullet\bullet}/2V_o^{\bullet} + \frac{1}{2}O_2 \quad (9)$$

where Vo, $Vo^{\bullet}$ and $Vo^{\bullet\bullet}$ represents oxygen vacancies which are neutral, singly ionized and doubly ionized. Oo is oxygen occupying oxygen lattice site. Mo/V_{Ti} is molybdenum or vanadium ion at titanium lattice site. V_{Ti} represents the titanium vacancies (which can be neutral or four times charged). The dot (•) represents the excess charge while the (′) represents the deficiency in the charge.

3.5 FTIR Analysis

FTIR spectra of TiO_2 and M-TiO_2 (M = Th^{4+}, V^{5+}, and Mo^{6+}) samples displayed strong absorption bands at 488 and 548 cm^{-1} which are characteristic peaks corresponding to anatase framework. The peaks at 3,426 and 1,654 cm^{-1} can be assigned to surface adsorbed water and hydroxyl groups [14]. M-TiO_2 (M = Th^{4+}, V^{5+}, and Mo^{6+}) samples had higher concentration of surface adsorbed water and hydroxyl groups compared to undoped TiO_2 which may be due to increase in the surface area of the samples. The peaks in the region 807–850 cm^{-1} are due to the peroxo vibrations of the type O–O. Further the peak at 660 cm^{-1} can be assigned to Ti–O–O in undoped TiO_2 sample. This peak shifts to 672 cm^{-1} for Mo^{6+} and

V^{5+} doped samples and 686 cm^{-1} for Th^{4+}-TiO_2 samples. This can be assigned to Ti–O–M bond.

3.6 SEM, EDX and BET Analysis

EDX analysis confirmed the incorporation of all the dopants in the TiO_2 lattice (Table 2), while SEM analysis showed the almost similar morphology for all the doped samples owing to the lower dopant concentration (Fig. 3). The surface areas for all the doped samples were greater than undoped samples due to the introduction of additional nucleation sites by the dopant which results in the increase of the surface area as confirmed by BET surface area analysis (Table. 1).

Table 2 EDX data for undoped TiO_2 and M-TiO_2 (M = Th^{4+}, V^{5+}, and Mo^{6+})

Dopant concentration (%)	Composition (atom %)					
	Th^{4+}-TiO_2		V^{5+}-TiO_2		Mo^{6+}-TiO_2	
	Ti	Th	Ti	V	Ti	Mo
0.02	97.87	2.13	97.92	2.08	98.06	1.94
0.06	94.2	5.88	93.98	6.02	94.02	5.98
0.1	88.98	11.02	90.05	9.95	90.25	9.75

3.7 Adsorption Studies

The amount of adsorption was calculated by comparing the concentration of IMC before (C_0) and after stirring (C) in the dark at pH 5.4. The percentage of adsorption was calculated from the $(1-C/C_0) \times 100$. IMC is a strong Lewis base due to the presence of pyridine ring and basic nitrogen atoms. At pH 5.4 the catalyst surface bears positive charge and acts as Lewis acid. Hence an electrostatic force of attraction between IMC and catalyst exists which renders the IMC adsorption on the catalyst surface. The decreasing adsorption capacity of the catalysts is of the order: Th^{4+}-TiO_2 (0.06%) > Th^{4+}-TiO_2 (0.1%) > Mo^{6+}-TiO_2 (0.06%) > V^{5+}-TiO_2 (0.06%) > Th^{4+}-TiO_2 (0.02%) > Mo^{6+}-TiO_2 (0.02%) > V^{5+}-TiO_2 (0.02%) > Mo^{6+}-TiO_2 (0.1%) > V^{5+}-TiO_2 (0.1%) > TiO_2. All the doped samples showed stronger adsorption capacities than undoped TiO_2.

3.8 Photo Degradation Experiments

Under solar light, sol–gel undoped TiO_2 (SG) was less effective to absorb photons due to its wide band gap and hence negligible degradation of IMC was observed. Degussa P-25 was able to degrade 31% attributed to the synergistic effect of the mixed phase and also smaller crystallite size of the sample. All the doped catalysts showed enhanced activity for the degradation compared to

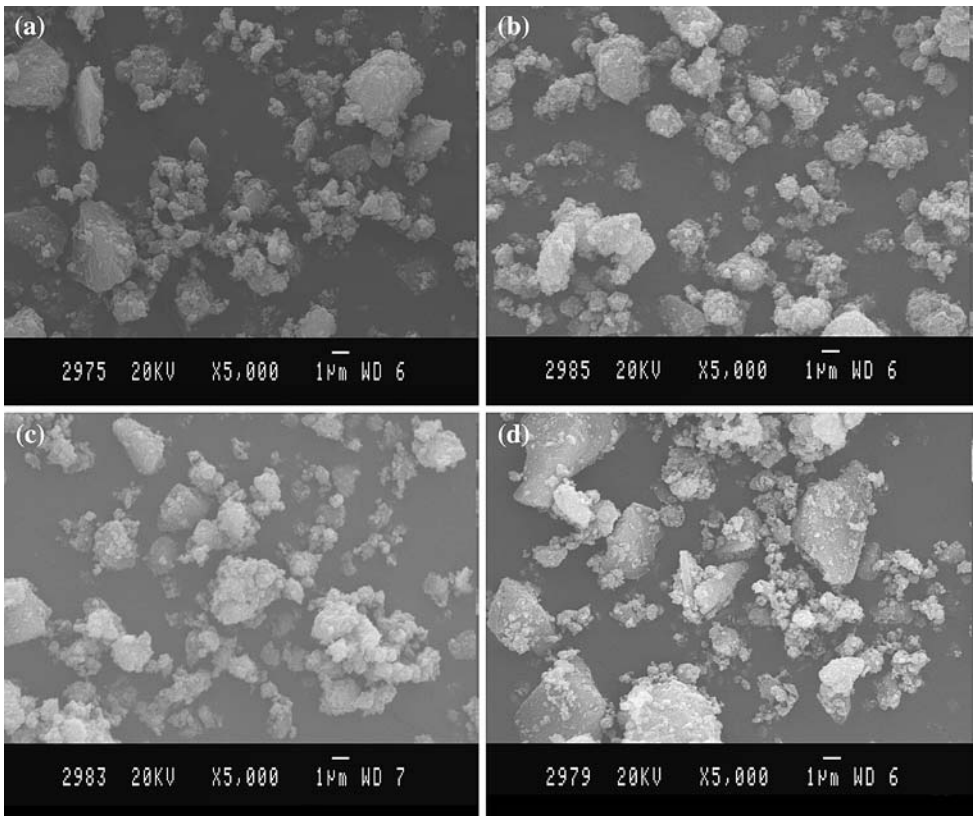

Fig. 3 SEM images of **a** undoped TiO_2; **b** Th^{4+} (0.06%)-TiO_2; **c** Mo^{6+} (0.06%)-TiO_2; **d** V^{5+} (0.06%)-TiO_2

TiO_2 (SG) and Degussa P-25 due to the lower band gap (Table 3). Among various doped catalysts used, Th^{4+} (0.06%)-TiO_2 showed better activity under solar light which is mainly due to the larger surface area of the sample, largest red shift and also may be due to the effective separation of charge carriers. Based on the experimental results obtained, it is proposed that the defect levels created by Th^{4+} ions in the TiO_2 lattice can capture the photo generated electrons and holes shallowly and detrap the same to adsorbed oxygen and hydroxyl ions, respectively, to generate super oxide and hydroxyl radicals. These processes not only suppress the recombination rate but can also generate the excess free radicals which are essential for the degradation reaction. The presence of vacant 'd' and 'f' orbitals in the Th^{4+}-TiO_2 sample are expected to behave as strong Lewis acid enhancing the adsorption of IMC (Lewis base) which could accelerate the interfacial charge transfer process [7]. The smaller crystallite size of the sample reduces the diffusion path length for the charge carriers from the site where they are photo produced, to the surface site where they possibly react. Reduction in this diffusion path length results in a reduced recombination rate of photo generated carriers and hence results in greater photo catalytic efficiency. In addition the induced oxygen vacancies in Th^{4+}-TiO_2 samples can efficiently capture the photo generated electrons thereby reducing the recombination rate. These oxygen vacancies enhance the process of adsorption of oxygen and increase the interaction between photoinduced electrons of oxygen vacancies and adsorbed oxygen. Thus oxygen vacancies and defects were in the favor of photo catalytic reactions leading to the mineralization of organic substances [15].

The plot of –log C/C_0 versus time showed that the degradation process followed first order kinetics in two stages for the doped catalysts (Fig. 4). The rate constant calculated for the second stage was greater than the first. Such behavior mainly depends on the structure of the pollutant and also on the nature of the photo catalysts. The structure of the IMC consists of pyridine ring and guanidine ring. The observed low rate constant in the first stage may be due to the difficulties in cleavage of IMC to pyridine and guanidine moieties (the formation of these intermediates were also confirmed by GC–MS technique). The subsequent reaction of the free radicals with pyridine and guanidine derivative is faster leading to the mineralization which results in higher rate constant in the second stage [3].

Table 3 Percentage degradation, process efficiency (Φ) and rate constant (k) of all the catalysts under solar light for the degradation imidachloprid

Photo catalysts	% degradation	Process efficiency (Φ) × 10^{-8}	Rate constant × 10^{-3} min^{-1}	
			I stage	II stage
TiO_2	5	0.60	0.12	0.21
Degussa P-25	35	4.23	1.44	1.75
Th-TiO_2 (0.02%)	76	9.19	3.68	7.33
Th-TiO_2 (0.06%)	100	12.1	5.37	16.31
Th-TiO_2 (0.1%)	85	10.28	4.21	10.91
V-TiO_2 (0.02%)	39	4.719	1.57	1.96
V-TiO_2 (0.06%)	45	5.44	1.81	2.62
V-TiO_2 (0.1%)	40	4.84	1.74	2.22
Mo-TiO_2 (0.02%)	70	8.47	3.35	6.04
Mo-TiO_2 (0.06%)	84	10.16	4.21	10.91
Mo-TiO_2 (0.1%)	76	9.07	3.68	7.33

Process efficiency $(\Phi) = \frac{(C_0 - C)}{tIS}$

C_0 is the initial concentration of the substrate and C is the concentration at time 't'

($C_0 - C$) concentration degraded in mg/L or ppm. 'I' is the irradiation intensity 125 W. 'S' denotes the solution irradiated plane surface area in cm^2 and 't' represents the irradiation time in minutes. It is expressed in ppm min^{-1} W^{-1} cm^{-2}

Rate constant is calculated from the plot of –log C/C_0 vs. time

3.9 Role of Dopants in TiO_2 Matrix

The dopants inside the matrix can serve as electron and hole traps. By considering the electronic configuration, variable oxidation state of the dopants and its oxidative capacity for the degradation of imidachlorid a probable mechanism for their behavior is shown below.1. If V^{5+} and

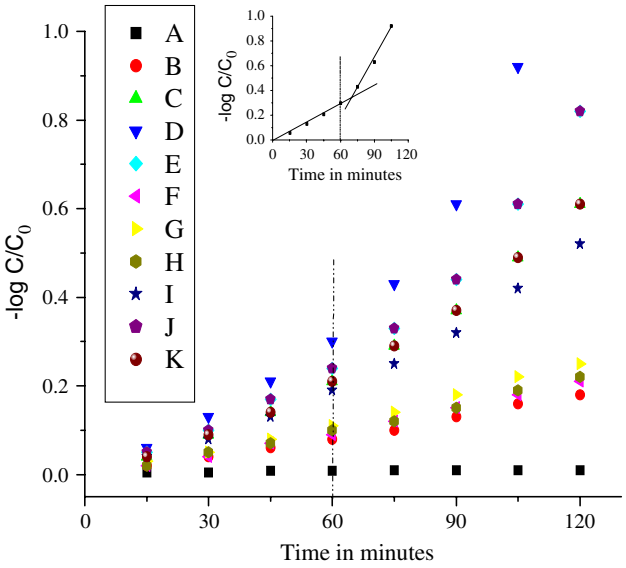

Fig. 4 Plot of –log C/C_0 vs. time for the degradation of pesticide using various photo catalysts under solar light. (*A*) TiO_2 (SG); (*B*) Degussa P-25; (*C*) Th^{4+}-TiO_2 (0.02%); (*D*) Th^{4+}-TiO_2 (0.06%); (*E*) Th^{4+}-TiO_2 (0.1%); (*F*) V^{5+}-TiO_2 (0.02%); (*G*) V^{5+}-TiO_2 (0.06%); (*H*) V^{5+}-TiO_2 (0.1%); (*I*) Mo^{6+}-TiO_2 (0.02%); (*J*) Mo^{6+}-TiO_2 (0.06%); (*K*) Mo^{6+}-TiO_2 (0.1%). The *inset plot* shows the two stage first order kinetics between intervals 0–60 and 90–120 min

Mo^{6+} are assumed to serve as electron traps, the possibility is

$$V^{5+} + e^- \rightarrow V^{4+} \quad (10)$$

$$Mo^{6+} + e^- \rightarrow Mo^{5+} \quad (11)$$

If V^{5+} and Mo^{6+} are assumed to serve as hole traps, then

$$V^{5+} + h^+ \rightarrow V^{6+} \quad (12)$$

$$Mo^{6+} + h^+ \rightarrow Mo^{7+} \quad (13)$$

The electronic configuration of V^{5+} is $3d^0\ 4\ s^0$ and Mo^{6+} is $4d^0\ 5\ s^0$ which are stable. When V^{5+} and Mo^{6+} traps conduction band electrons their electron configuration will be $3d^0\ 4\ s^1$ and $4d^0\ 5\ s^1$, respectively, which are unstable. Therefore it possibly transfers the trapped electron to adsorbed oxygen on the catalyst surface which generates highly oxidative superoxide radicals.

$$V^{4+} + O_{2ads} \rightarrow V^{5+} + O_2{}^{-\bullet} \quad (14)$$

$$Mo^{5+} + O_{2ads} \rightarrow MO^{6+} + O_2{}^{-\bullet} \quad (15)$$

Since the existence of vanadium in +6 and molybdenum in +7 oxidation state are also highly unstable. It transfers the hole to the adsorbed hydroxyl groups on the catalyst surface at a much faster rate compared to the transfer of the trapped electrons.

$$V^{+6} + OH^- \rightarrow V^{+5} + OH^{\bullet} \quad (16)$$

$$Mo^{7+} + OH^- \rightarrow Mo^{6+} + OH^{\bullet} \quad (17)$$

The thorium has only one stable oxidation state of +4 with electronic configuration of $6^0_d\ 5^0_f$. Though it traps conduction band electron or valence band hole it can detrap the same to the catalyst surface at a much faster rate to restore its stable electronic configuration with vacant 'f' and 'd' orbital compared to the V^{5+} and Mo^{6+} which has only vacant d orbital. This may probably account for the highest enhanced activity of Th-TiO_2 (0.06%) under sunlight.

$$Th^{4+} + e^- \rightarrow Th^{3+} \quad (18)$$

$$Th^{3+} + O_{2ads} \rightarrow Th^{4+} + O_{2ads}{}^{-\bullet} \quad (19)$$

$$Th^{4+} + h^+ \rightarrow Th^{5+} \quad (20)$$

$$Th^{5+} + OH^- \rightarrow Th^{4+} + OH^{\bullet} \quad (21)$$

Therefore we can conclude that the dopant effectiveness lies not only in trapping the charge carriers to prevent recombination reactions but it should also detrap the charge carriers thereby facilitating the generation of highly reactive oxidative radicals like hydroxyl and super oxide radicals which accelerates the interfacial charge transfer process. Further the detrapping of the charge carriers mainly depends on the oxidation state and stable electronic configuration of the dopant.

4 Conclusion

A series of metal ion doped M-TiO_2 (M = Th^{4+}, V^{5+}, and Mo^{6+}) were prepared and photo catalytic activities of these catalysts were tested for the degradation of imidachloprid pesticide under solar light and the results were compared with Degussa P-25. Th^{4+} (0.06%)-TiO_2 showed enhanced activity under solar light compared to all the other catalysts used. The presence of vacant d and f orbitals in the thorium ion behaves as strong Lewis acid which increases the adsorptive capacity of imidachloprid which is a Lewis base. Further the observed large shift in the absorption band (486 and 466 nm) is due to the creation of mid band gap states by the dopants and also due to its small crystallite size which additionally enhances the degradation process. Based on the experimental results probable role played by the dopant ions in the TiO_2 matrix is explained. It is suggested that the dopant effectiveness lies not only in trapping the charge carriers to prevent recombination reactions but it should also detrap the charge carriers at a faster rate to facilitate the generation of highly reactive oxidative radicals like hydroxyl and super oxide radicals. The detrapping of the trapped charge carriers depends mainly on the electronic configuration and stable oxidation state of the dopants.

Acknowledgments Financial assistance from UGC Major Research Project (2007–2010), is acknowledged. The author B. Narasimha Murthy acknowledges to C.M.R. Institute of Technology for their support.

References

1. Bahnemann W, Muneer M, Haque MM (2007) Catal Today 124:133
2. Li Puma G, Toepfer B, Gora A (2007) Catal Today 124:124
3. Wang XH, Li JG, Kamiyama H, Moriyoshi Y, Ishigaki T (2006) J Phys Chem B 110:6804
4. Gomathi Devi L, Narasimha Murthy B (2008) Catal Lett 125:320
5. Xu A-W, Gao Y, Liu H-Q (2002) J Catal 207:151
6. Li FB, Li XZ, Hou MF, Cheah KW, Choy WCH (2005) Appl Catal A Gen 285:181
7. Ranjit KT, Willner I, Bossmann SH, Braun AM (2001) Environ Sci Technol 35:1544
8. Gomathi Devi L, Krishnaiah GM (1999) J Photochem Photobiol A Chem 121:141
9. Lin J, Yu JC (1998) J Photochem Photobiol A Chem 116:63
10. Burns A, Hayes G, Li W, Hirvonen J, Derek Demaree J, Ismat Shah S (2004) Mater Sci Eng B 111:150
11. Breuer HD, Wilke K (1999) J Photochem Photobiol A Chem 121:49
12. Sanchez E, Lopez T (1995) Mater Lett 25:271
13. Hur SG, Kim TW, Hwang SJ, Park H, Choi W, Kim SJ, Choy JH (2005) J Phys Chem B 109:15001
14. Ding Z, Lu Q, Green Field PF (2000) J Phys Chem B 104:4815
15. Xiao Q, Si Z, Yu Z, Qiu G (2008) J Alloy Compd 450:426